

Polarization dependence of phonon influences in exciton-biexciton quantum dot systems

M. Glässl^{1*} and V. M. Axt¹

¹*Institut für Theoretische Physik III, Universität Bayreuth, 95440 Bayreuth, Germany*

(Dated: July 28, 2018)

We report on a strong dependence of the phonon-induced damping of Rabi dynamics in an optically driven exciton-biexciton quantum dot system on the polarization of the exciting pulse. While for a fixed pulse intensity the damping is maximal for linearly polarized excitation, it decreases with increasing ellipticity of the polarization. This finding is most remarkable considering that the carrier-phonon coupling is spin-independent. In addition to simulations based on a numerically exact real-time path integral approach, we present an analysis within a weak coupling theory that allows for analytical expressions for the pertinent damping rates. We demonstrate that an efficient coupling to the biexciton state is of central importance for the reported polarization dependencies. Further, we discuss influences of various system parameters and show that for finite biexciton binding energies Rabi scenarios differ qualitatively from the widely studied two-level dynamics.

I. INTRODUCTION

Investigations devoted to the carrier dynamics of optically driven quantum dots (QDs) with or without an additional coupling to a cavity constitute a highly active field of physics.^{1–11} In the limit of strong electronic confinement and for excitations with arbitrarily polarized laser pulses, the electronic structure of a QD can be modeled as a four-level system, consisting of the ground state (no electron-hole pair), two energetically almost degenerate single exciton states with orthogonal spin polarizations and the biexciton state. Such exciton-biexciton systems are attractive for many innovative technologies, including the realization of sources for on-demand entangled or squeezed photons^{12–15} or applications in the field of quantum information theory.^{16–18} The major obstacle for coherent manipulations is decoherence, and much effort has been devoted to characterize or minimize decoherence processes in optically driven QDs.^{3–6,11,19–27} Recent experimental studies of excitonic Rabi rotations^{4,5} identified the pure dephasing coupling of carrier states to bulk like acoustic phonons as the principal source of dephasing in self-assembled QDs and confirmed theoretically predicted results for phonon-coupled two-level systems, such as a renormalization of the Rabi frequency.^{22,24} Moreover, first evidence for the expected undamping of Rabi rotations at high pulse areas^{3,28} has been shown by observing a roll-off behavior in the oscillation amplitude.⁵

Obviously, the dissipative dynamics of a four-level system accounting not only for single exciton but also for biexciton excitations can develop much more manifold than that of a two-level system and is in view of possible applications of special interest. Most of the existing literature on the phonon impact on the carrier dynamics of optically driven QDs, however, deals with electronic two-level systems and comparatively little is known about the more complex exciton-biexciton dynamics. In Refs. 29 and 30 analytic expressions have been derived for the limit of ultrashort excitations. Two-photon Rabi oscil-

lations between the ground and the biexciton state have been studied experimentally in Ref. 31 and the phonon influence on this scenario has been analyzed theoretically within a perturbative approach in Ref. 32. Very recently, we have demonstrated that a numerically exact real-time path integral approach previously used for two-level systems^{3,28,33} can be also implemented for four-level systems paving the way towards investigations in the regimes of high temperatures, strong carrier-phonon couplings and long times for arbitrary optical drivings.³⁴ In that work dark superpositions were identified as a general mechanism that strongly modifies the quantum dissipative relaxation, in particular at long times, and various related dynamical features have been discussed, including a crossover between two qualitatively different relaxation scenarios.³⁴

Here, we analyze in detail the impact of acoustic phonons on the dynamics on shorter time-scales than in Ref. 34 concentrating on Rabi scenarios and signals most convenient to be studied in experiments. In particular, we study the dynamics for different intensities and polarizations of the driving laser field. As the exciton-phonon coupling is independent of the spin, it might be suspected, that the phonon influence does not depend on the polarization of the optical excitation which creates well defined superpositions of carrier spins. Nevertheless, we shall demonstrate that in contrast to this expectation, the phonon-induced damping does strongly depend on the polarization of the exciting pulse. Keeping the pulse intensity fixed, the damping is most pronounced for linear polarization, while for elliptical polarizations it becomes the more reduced the closer the polarization is to the circular limit.

The paper is organized as follows. In Sec. II we introduce the model, we present a short summary of the path integral approach used and comment on the challenges that are faced when accounting for four electronic levels within this numerically exact formalism. In addition, we introduce a weak coupling theory that allows for approximate but explicit expressions for the pertinent damping rates. This perturbative approach is described in more

detail in the appendix and most clearly reveals the origin of the polarization dependence of the phonon-induced damping. The latter is presented in Sec. III, where we also study in detail the dynamics for linearly polarized excitations and discuss the influence of pulse intensity, temperature and magnitude of the biexciton binding energy. Special emphasis is put on comparisons with results for two-level systems. Finally, we summarize our results in Sec. IV.

II. THEORY

A. Model

We consider a strongly confined GaAs QD with spin degenerate electronic particle states coupled to a continuum of acoustic phonons and driven by laser light. The corresponding Hamiltonian can be written as

$$H = H_{\text{dot}} + H_{\text{ph}} + H_{\text{dot-ph}} + H_{\text{dot-light}}, \quad (1)$$

where H_{dot} describes the electronic structure of the QD, H_{ph} is the free phonon Hamiltonian, $H_{\text{dot-ph}}$ represents the carrier-phonon and $H_{\text{dot-light}}$ the carrier-light coupling. As in the strong confinement limit the electronic single particle states are energetically well separated, we can safely neglect a Coulomb-induced mixing of states with different single particle energies and concentrate on the topmost valence and lowest conduction band states. Neglecting excitonic states that are not coupled to other electronic states via the carrier-light interaction, our system comprises four states. Besides the ground state $|G\rangle$ without electron-hole pairs we account for the two single exciton states $|+\rangle$ and $|-\rangle$ with a total angular momentum of ± 1 , and the biexciton state $|B\rangle$. Then, H_{dot} reads

$$H_{\text{dot}} = \hbar\Omega (|+\rangle\langle +| + |-\rangle\langle -|) + (2\hbar\Omega - \Delta) |B\rangle\langle B| + V_{\text{ex}} (|+\rangle\langle -| + |-\rangle\langle +|). \quad (2)$$

We take the unexcited ground state as the zero of energy, $\hbar\Omega$ defines the ground state exciton transition energy, Δ denotes the biexciton binding energy resulting from electrostatic Coulomb interactions and V_{ex} the electron-hole exchange interaction. For simplicity, we consider spherical dots with envelope functions given by the ground state solution of a harmonic potential, i. e.

$$\psi_{e(h)}(r) = \frac{1}{\pi^{3/4} a_{e(h)}^{3/2}} \exp\left(-\frac{r^2}{2a_{e(h)}^2}\right), \quad (3)$$

where $a_{e(h)}$ denote the localization lengths of electrons and holes, respectively.

To model the carrier-phonon interaction we concentrate on pure dephasing couplings^{19,35} of the electronic states to bulk like longitudinal acoustic (LA) phonons via the deformation potential that for strongly confined GaAs QDs has been identified as the dominant dephasing

mechanism^{4,21}. With $b_{\mathbf{q}}^\dagger$ denoting the creation operator of a LA phonon with wave vector \mathbf{q} and energy $\hbar\omega_{\mathbf{q}}$, H_{ph} and $H_{\text{dot-ph}}$ are then given by

$$H_{\text{ph}} = \hbar \sum_{\mathbf{q}} \omega_{\mathbf{q}} b_{\mathbf{q}}^\dagger b_{\mathbf{q}}, \quad (4)$$

$$H_{\text{dot-ph}} = \sum_{\mathbf{q}} \sum_{\nu} (\gamma_{\mathbf{q}}^* b_{\mathbf{q}} + \gamma_{\mathbf{q}} b_{\mathbf{q}}^\dagger) n_{\nu} |\nu\rangle\langle \nu|. \quad (5)$$

The dispersion is assumed to be linear, $\omega_{\mathbf{q}} = v_c |\mathbf{q}|$, where $v_c = 5110$ m/s is the sound velocity, n_{ν} is the number of electron-hole pairs present in the state $|\nu\rangle$ (i. e., $n_G = 0$, $n_+ = n_- = 1$ and $n_B = 2$) and $\gamma_{\mathbf{q}}$ denote the exciton-phonon coupling constants. We stress, that the carrier-phonon coupling as given in Eq. (5) is independent of the carrier spin. Besides, it should be noted that the factorization in Eq. (5) into a product of $\gamma_{\mathbf{q}}$ and n_{ν} is valid for strongly confined QDs, where it is justified to treat excitons and biexcitons as product states representing uncorrelated electron-hole pairs. However, this factorization does not hold in general. For QDs far from the strong confinement limit, e. g., interface QDs, measurements³⁶ indicate strong deviations from Eq. (5). Details on the phonon coupling can be found in Ref. 19.

Finally, the coupling to the light field reads within the common dipole and rotating wave approximation

$$H_{\text{dot, light}} = -\hbar [F_{\sigma_+}(t) (|+\rangle\langle G| + |B\rangle\langle -|) + F_{\sigma_-}(t) (|-\rangle\langle G| + |B\rangle\langle +|) + \text{h.c.}], \quad (6)$$

where $F_{\sigma_{\pm}} = \mathbf{E}_{\sigma_{\pm}}^{(+)}(t) \mathbf{M} / \hbar$ with $\mathbf{E}_{\sigma_{\pm}}^{(+)}(t)$ being the positive frequency part of the σ_{\pm} circularly polarized component of the light field and \mathbf{M} denoting the ground state exciton transition dipole moment, that we assume to be identical to the exciton biexciton transition dipole moment. Taking the laser frequency to be in resonance with the polaron shifted exciton transition frequency $\bar{\Omega} = \Omega - \sum_{\mathbf{q}} \gamma_{\mathbf{q}}^2 / \omega_{\mathbf{q}}$, we set $F_{\sigma_{\pm}}(t) = f_{\sigma_{\pm}}(t) \exp(-i\bar{\Omega}t) / 2$ with real envelope functions $f_{\sigma_{\pm}}(t)$, that we will refer to as σ_{\pm} circularly polarized field strengths. The total field strength is given by $f(t) = \sqrt{f_{\sigma_+}^2(t) + f_{\sigma_-}^2(t)}$ and defines the pulse area α of an applied laser pulse via

$$\alpha = \int_{-\infty}^{\infty} f(t) dt. \quad (7)$$

For linearly polarized laser pulses, the total pulse intensity is equally distributed between both circularly polarized components, i. e., $f_{\sigma_+} = f_{\sigma_-} = f / \sqrt{2}$, and both spin degenerate excitons experience the same dynamics. For circularly polarized pulses with $f = f_{\sigma_{\pm}}$ and $f_{\sigma_{\mp}} = 0$, the system reduces for $V_{\text{ex}} = 0$ to an effective two-level system. All other polarizations we will refer to as elliptical. Note, that the definition of the pulse area in Eq. (7) is such, that for circular polarizations (i.e., a two-level model), a pulse area of $\alpha = \pi$ inverts the system.³⁷

B. Path integral approach

To study the combined carrier-phonon dynamics, we use a real-time path integral approach, that for the four-level system has first been applied in Ref. 34. This approach is numerically exact in the sense that there are no approximations within the model given above, and thus we face no errors beyond well controllable discretization errors. The reduced electronic density matrix is calculated by taking the Liouville von Neumann equation for the full density matrix and tracing over the phonon degrees of freedom, where the time evolution operator is represented as a path integral. Tracing out the phonon degrees of freedom introduces a memory and leads to a non-Markovian dynamics for the reduced density matrix, that can be fully accounted for. A complete description of our algorithm can be found in Ref. 38, where we give not only a detailed derivation, but highlight also specifics of our implementation that are related to the superohmic character of the carrier-phonon coupling and that are not encountered in implementations of path integrals for studies with ohmic or subohmic coupling types.^{39–42}

The numerically complete treatment within the path integral approach rapidly becomes ambitious, when more than two electronic levels are taken into account. As explained in Ref. 38, the number of paths that have to be considered is given by $L^{2(n_c+1)}$, where L is the number of electronic levels (i.e., here $L = 4$) and n_c the number of retarded time steps that are accounted for. Obviously, keeping n_c fixed, the number of paths is squared when one accounts for four instead of two electronic levels, and thus the numerical effort increases drastically. A reduction of the number of paths can be achieved by invoking an on-the-fly path selection as described in Ref. 38 and first introduced by Sim.⁴³ This enables studies with a sufficiently fine time discretization but at the price of enforcing additional convergence tests, that have to be performed individually for different parameter ranges.

C. Weak Coupling Theory

In order to better understand the origin of the polarization dependence of the phonon-induced damping and some other features to be presented in Sec. III, we set up equations of motion for the reduced electronic density matrix within a weak coupling theory⁴⁴. A more detailed description of this perturbative approach that is essentially equivalent to a standard Born-Markov master equation approach⁴⁵ is given in the appendix. Here, we shall only give a short summary.

First, we transform H as given in Eqs. (1)-(6) from the electronic basis $\{|G\rangle, |+\rangle, |-\rangle, |B\rangle\}$ to the basis spanned by the instantaneous eigenstates of $H_{\text{dot}}+H_{\text{dot-light}}$, that are usually referred to as dot-photon dressed states. To keep the formulas as simple as possible, we concentrate on the special case $\Delta = V_{\text{ex}} = 0$. For this choice, the dressed states are independent on $f_{\sigma_{\pm}}$ as well as on time

and given by $\mathbf{d}_1 = (1, 1, 1, 1)$, $\mathbf{d}_2 = (1, 1, -1, -1)$, $\mathbf{d}_3 = (1, -1, -1, 1)$ and $\mathbf{d}_4 = (1, -1, 1, -1)$ with corresponding eigenenergies $-\hbar\lambda_j$, where $\lambda_1 = f_+$, $\lambda_2 = f_-$, $\lambda_3 = -f_+$, $\lambda_4 = -f_-$ and $f_{\pm} = (f_{\sigma_{\pm}} \pm f_{\sigma_{\mp}})/2$.

Setting up equations of motion for the reduced electronic density matrix $\rho_{ij} = \langle |d_i\rangle \langle d_j| \rangle$ leads to a hierarchy of phonon assisted quantities, that we truncate by factorizing at the level of two phonon assistances. Next, we integrate the one phonon assisted density matrix elements performing a Markov approximation and substitute the resulting expressions back into the equation for the reduced density matrix. Transforming back to the electronic basis $\{|G\rangle, |+\rangle, |-\rangle, |B\rangle\}$ yields for example:

$$\begin{aligned} \partial_t \rho_{12} = & i/2 [f_{\sigma_+} (\rho_{11} - \rho_{22}) + f_{\sigma_-} (\rho_{14} - \rho_{32})] \\ & + \pi/4 [J(f_{\sigma_+}) (\rho_{11} + \rho_{22}) - J(f_{\sigma_-}) (\rho_{14} - \rho_{32})] \\ & - \pi/2 J(f_{\sigma_+}) \coth(\hbar f_{\sigma_+}/2kT) \rho_{12}, \end{aligned} \quad (8)$$

where we have introduced the phonon spectral density

$$J(\omega) = \sum_{\mathbf{q}} \gamma_{\mathbf{q}}^2 \delta(\omega - \omega_{\mathbf{q}}). \quad (9)$$

The main purpose for deriving the above approximate equations in addition to our numerically complete treatment within the path integral formalism is to obtain simple closed form expressions for the relevant damping rates in terms of the phonon spectral density that allow for an explicit discussion of the dependencies on the field components $f_{\sigma_{\pm}}$. The field strengths enter the damping rates because the energy conservation condition, that occurs in the Markov limit, enforces the phonon frequency to match the difference between electronic dressed state energies $E_j = -\hbar\lambda_j$, which are directly related to $f_{\sigma_{\pm}}$. Therefore, the phonon spectral density $J(\omega)$ is evaluated at the corresponding transition frequencies. For the special case $\Delta = V_{\text{ex}} = 0$ discussed here, it is important to note that $J(\omega)$ is only evaluated at f_{σ_+} and f_{σ_-} [cf. Eq. (8) as an example], i.e., it is the strength of the σ_+ and the σ_- component separately, and not the total intensity, that matters.

III. RESULTS

In the following we will study the electronic dynamics that result from the interplay between optical excitation and the phonon-induced dephasing. For our calculations, that have been performed using the path integral approach, we choose $a_e = 4$ nm, we set $a_h = 0.87a_e$, and assume that initially, the QD is in the unexcited ground state and the phonons in a thermal state at temperature T . Δ and V_{ex} are treated as parameters. In Sec. III A we concentrate on linearly polarized excitations and investigate how the laser pulse intensity affects the dynamics. Here, a special focus is put on comparing the results with those of the widely studied two-level model, where biexcitonic excitations are not accounted for. Sec. III B

is devoted to the case of elliptically polarized excitations and the polarization dependence of the phonon influence.

A. Linearly Polarized Excitations

Let us first concentrate on linearly polarized excitations ($f_{\sigma_+} = f_{\sigma_-}$) and consider the Rabi rotation scenario, where the final occupation after the pulse is recorded as a function of the applied pulse area α as given in Eq. (7) which is most convenient to be studied in experiments. Fig. 1 shows corresponding results for the ground state occupation $C_G = \rho_{11}$ (green dashed line), the total single exciton occupation $C_E = \rho_{22} + \rho_{33}$ (red dotted line), and the biexciton occupation $C_B = \rho_{44}$ (blue solid line) for a rectangular 12 ps lasting pulse at different temperatures for $\Delta = V_{\text{ex}} = 0$. In the phonon-free case [Fig. 1(a)], the occupations of the ground and biexciton state perform undamped oscillations between 0 and 1 with a period of $2\sqrt{2}\pi$, while the total single exciton occupation does not take values above 0.5 and oscillates twice as fast. Recall, that the definition of the pulse area has been chosen such, that for a two level system the occupation oscillates with a period of 2π and that for linearly polarized excitations $f_{\sigma_{\pm}} = f/\sqrt{2}$, explaining the additional factor $\sqrt{2}$ that enters the period of the ground and biexciton state occupation. Accounting for the carrier-phonon interaction yields a damping and a renormalization of the Rabi period. As shown in Figs. 1(b)-1(d) both effects strongly depend on temperature. Qualitatively similar results have previously been reported for electronic two-level systems^{22,24,28,46}.

The probably most striking theoretical prediction for the dissipative two-level dynamics is that the phonon-induced damping should depend nonmonotonically on the pulse intensity resulting in a reappearance of Rabi rotations at high pulse areas^{28,38}. Recently, first experimental evidence for this reappearance has been reported⁵ for QDs driven by circularly polarized light, where a two-level model can be applied: the measured data showed a clear roll-off behaviour at high pulse areas. Of course, the question arises as to how this scenario appears for linear polarization, in particular for finite values of the biexciton binding energy, and which differences can be expected compared to the two-level case. To answer these questions, different Rabi rotation scenarios are presented in Fig. 2 for a 12 ps lasting rectangular pulse at $T = 10$ K. The rectangular pulse shape, that in experiments can be realized applying well known pulse-shaping techniques⁴⁷, has been chosen as for such pulses the reappearance is more pronounced than for bell-shaped pulses²⁸.

Shown in Fig. 2(a) are Rabi rotations for $\Delta = V_{\text{ex}} = 0$. While for small pulse areas the damping increases with rising pulse intensity (as also seen in Fig. 1), it decreases at high pulse areas resulting in a reappearance of Rabi rotations. The pulse area α_c with minimal Rabi rotation amplitude is the same for C_G , C_E and C_B and for the chosen parameters roughly given by $\alpha_c = 11\pi$. We stress

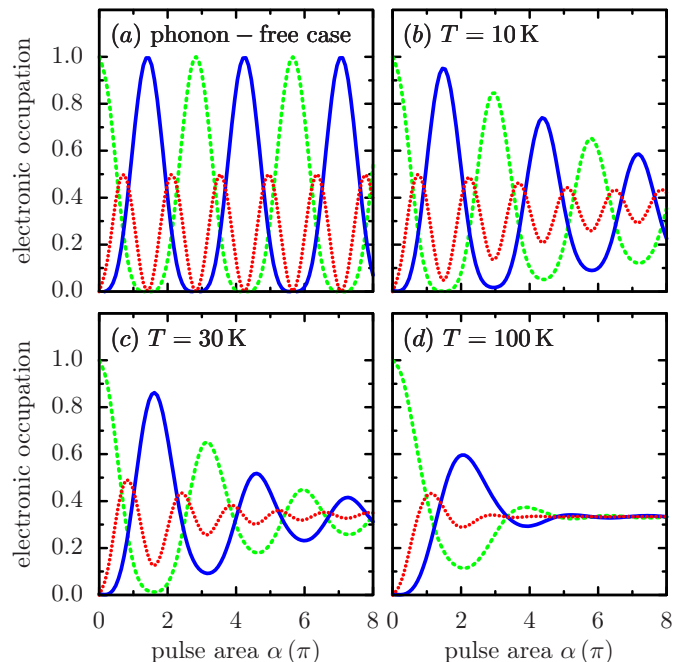


FIG. 1: (Color online) Occupation of the ground state C_G (green dashed line), the total single exciton occupation C_E (red dotted line), and the biexciton occupation C_B (blue solid line) as a function of the applied pulse area α for a linearly polarized rectangular pulse of 12 ps duration and $\Delta = V_{\text{ex}} = 0$. (a) Displays results for the phonon-free case, (b)-(d) show the dynamics in the full model at temperatures of (b) $T = 10$, (c) 30, and (d) 100 K.

that the reappearance of Rabi rotations is different from the collapse and revival phenomenon within the Jaynes-Cummings model⁴⁸, which describes the temporally periodic carrier dynamics of a two-level system coupled to a single-mode quantized photon field. For the system considered here, the oscillation amplitudes of all occupations decay monotonically with time, but with a damping depending nonmonotonically on the applied pulse area. The physical origin of this nonmonotonic damping, that is reflected in an undamping of Rabi rotations at high pulse areas, is the resonant nature of the carrier-phonon interaction²³: the exciton-phonon coupling is maximal at intermediate pulse areas, where the frequencies of the electronic oscillations are resonant with the most strongly coupled lattice modes.

In experimental studies, the final QD occupation after a pulse is often measured using a photocurrent detection technique,^{4,49,50} where under the action of an applied electric field, the carriers, that have been created during the exciting pulse, tunnel from the QD resulting in a photocurrent. For an exciton-biexciton system, this photocurrent is proportional to the weighted sum $C := C_E + 2C_B$ of the generated single exciton and biexciton populations. In the following, we will concentrate on this total electronic occupation instead of the single contributions C_E or C_B that in experiments are much

harder to extract individually.

Plotted in Fig. 2(b) is $C/2$ for $\Delta = V_{\text{ex}} = 0$ (thick black line) together with the exciton occupation $C_{2\text{LS}}$ of a two-level system (thin red line), that for $V_{\text{ex}} = 0$ we can model by choosing circularly polarized laser light. For the four-level case, the maximal signal is not only twice as high as in the two-level case (mind the scaling factor of 0.5 for C) but the pulse area with minimal amplitude, marking the beginning of the reappearance, is also considerably higher. This difference can be understood with the help of Eq. (8): the phonon-induced damping is expressed in terms of the phonon spectral density $J(\omega)$ that rises for small frequencies and peaks at a certain frequency $\bar{\omega}$ before it eventually decreases^{26,38}. The important point to note is that for the chosen parameters J is not evaluated at the total field strength f but at the circularly polarized field strengths f_{σ_+} and f_{σ_-} (which are identical for linear polarization). Further, for a given pulse area α , the circularly polarized field strengths of a linearly polarized pulse are by a factor of $\sqrt{2}$ smaller than the field strength of a circularly polarized pulse. Thus, to reach the field strength, where J and thereby the phonon-induced damping is maximal, higher pulse areas are needed for linearly polarized pulses than for circularly polarized pulses and hence, the reappearance starts later in the linear case. For the same reason, higher pulse areas are needed to fully restore the maximal Rabi rotation amplitude.

Next, in Fig. 2(c), we shall discuss the influence of the biexciton binding energy, which, depending on details of the quantum dot geometry, may take negative as well as positive values. While for $\Delta = 0$ (black dotted line) the dependence of C on α is similar to that of the two-level case, Rabi scenarios become much more complex for finite biexciton binding energies, where they qualitatively differ from the two-level results. For $\Delta = -1.0$ (blue solid line) or $+1.0$ meV (blue dashed line) there is still a reappearance in the sense that first the Rabi rotation amplitude decreases with increasing pulse area before it eventually rises again, but in contrast to $\Delta = 0$ the signal consists of a superposition of different transition frequencies and the mean value varies with α . For small pulse areas, the mean value is less than one and the signal does almost not depend on the sign of Δ . For intermediate pulse areas, it increases and we observe a pronounced difference between $\Delta = -1.0$ and $+1.0$ meV, whereas for high pulse areas, both binding energies result again in similar oscillations with a mean value of approximately one. Further, there is a clearly visible increase of the oscillation period with rising pulse areas.

To understand these features, it is helpful to consider the biexciton contribution $2C_B$ to the total photocurrent as shown in Fig. 2(d). For small pulse areas, the driving field strengths $f_{\sigma_{\pm}}$ are much smaller than $|\Delta/\hbar|$. From analytic expressions for driven two-level systems without a coupling to phonons³⁷, it is well known that off-resonant transitions become unlikely, when the frequency detuning is larger than the driving field strength and that

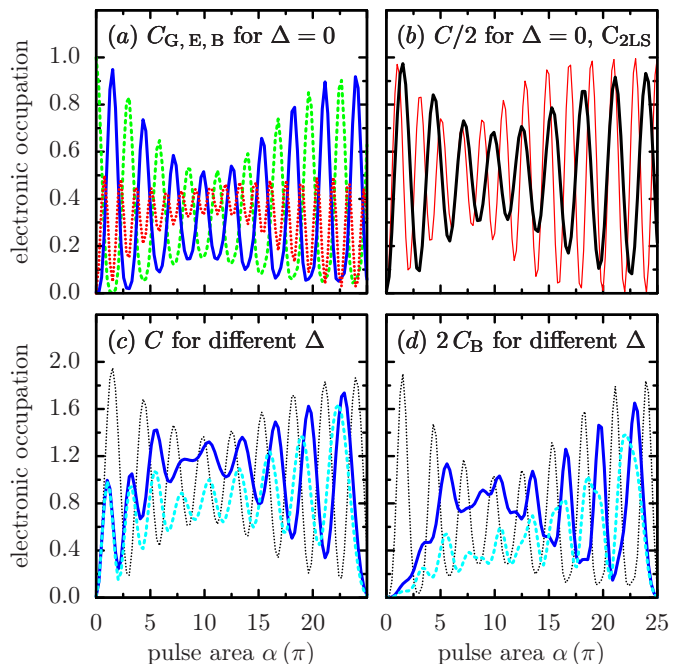


FIG. 2: (Color online) Rabi rotation scenarios at $T = 10$ K for a linearly polarized rectangular pulse of 12 ps duration. (a) C_G (green dashed line), C_E (red dotted line), and C_B (blue solid line) for $\Delta = 0$ meV. (b) Total electronic occupation $C = C_E + 2C_B$ (thick black line) and corresponding result for a two-level system (red thin line, see text). (c) $C = C_E + 2C_B$ for $\Delta = 0$ (black dotted line), $+1.0$ (blue solid line), and -1.0 meV (blue dashed line). (d) Biexciton contribution $2C_B$ to the signals plotted in (c) for the same parameters as there.

the dynamics does not depend on the sign of the detuning. Accounting for phonons, these statements remain approximately valid as long as the time-scales considered are much shorter than the time-scale, on which the system is driven to a stationary state³³, which is fulfilled for small pulse areas. Thus, the biexciton is hardly excited [cf. Fig. 2(d)] in the regime of low pulse intensities and C basically given by C_E . With increasing pulse area, the generation of the biexciton becomes more and more likely and C_B starts to contribute, which is reflected in an increase of the mean value of C . At intermediate pulse areas, the contribution of C_B is noticeable but depends strongly on the sign of Δ . The latter can be explained as follows: as already mentioned above, the carrier-phonon interaction is maximal at intermediate pulse areas, where the system is quite rapidly driven to a stationary non-equilibrium state. As shown in Ref. 34, the stationary occupations depend on the question whether dark superposition states are realized or not and are also strongly dependent on Δ and T . For the given temperature of $T = 10$ K and a driving field strength of $f = 2.0 \text{ ps}^{-1}$ [corresponding to pulse areas for which the Rabi rotation amplitude is minimal in Fig. 2(c)], the stationary biexciton occupation is roughly 0.55 for $\Delta = 1$ meV, while for $\Delta = -1.0$ meV it is strikingly less and roughly given by

0.14. Although we never reach a stationary state within the considered pulse duration of 12 ps, fingerprints of the relaxation process become visible in the regime of an enhanced carrier-phonon interaction as given at intermediate pulse areas and lead to the strong dependence on the sign of Δ . At high pulse areas, the driving field strengths are eventually significantly larger than $|\Delta/\hbar|$, the biexciton can be efficiently excited and due to the decreasing phonon influence with increasing pulse area the system is more and more far from becoming stationary, which results in a diminishing dependence on the sign of Δ . Finally, the increasing period of the oscillations of C with rising α can be explained by the increasing contribution of C_B that shows a considerably longer period than C_E as already discussed in Fig. 1 and also shown in Fig. 2(a).

B. Elliptically Polarized Excitations

So far, we have studied the exciton-biexciton dynamics under linearly polarized pulses. It was shown that the coupling between carriers and phonons strongly depends on the pulse intensity and that Rabi rotation scenarios for finite Δ are qualitatively different from those of two-level models, while they are similar for $\Delta \sim 0$. In what follows, we shall demonstrate a remarkable polarization dependence of the phonon-induced damping in an exciton-biexciton system, which has obviously no analogue in a two-level system.

To quantify the ellipticity of the polarization, we first introduce a polarization parameter γ via $f_{\sigma_-} = \gamma f_{\sigma_+}$. For $\gamma = 1$, we obtain linearly polarized light, while a circularly polarized excitation is realized for $\gamma = 0$. Plotted in Fig. 3(a) is the total electronic occupation $C = C_E + 2C_B$ as a function of time under cw-excitation for polarization parameters with $\gamma = 1$ (black dashed line), 0.5 (red solid line), 0.3 (green dotted line), and 0.1 (blue dashed-dotted line), respectively. The total field strength has been fixed to $f = 2.0 \text{ ps}^{-1}$, i.e., the pulse intensity is the same for all displayed results, and we have chosen a vanishing biexciton binding energy Δ as well as a vanishing exchange interaction V_{ex} , as for $\Delta = V_{\text{ex}} = 0$ an interpretation based on the simple rates derived in Sec. II C for this case can be made. For all excitation conditions, the total electronic occupation performs damped Rabi oscillations. But remarkably, the phonon-induced damping strongly depends on the polarization of the excitation. While the damping is strongest for linearly polarized light, the signal is the less damped the closer the polarization is to be circular. For $\gamma = 0.1$, corresponding to an almost circularly polarized excitation, the oscillation amplitude is after 50 ps more than 15 times larger than for linear polarization ($\gamma = 1$), where the oscillation amplitude is after 50 ps strongly reduced and the system already close to becoming stationary. As the carrier-phonon coupling as given by $H_{\text{dot-ph}}$ is identical for σ_+ and σ_- excitons, a polarization dependent damping of Rabi rotations is at first

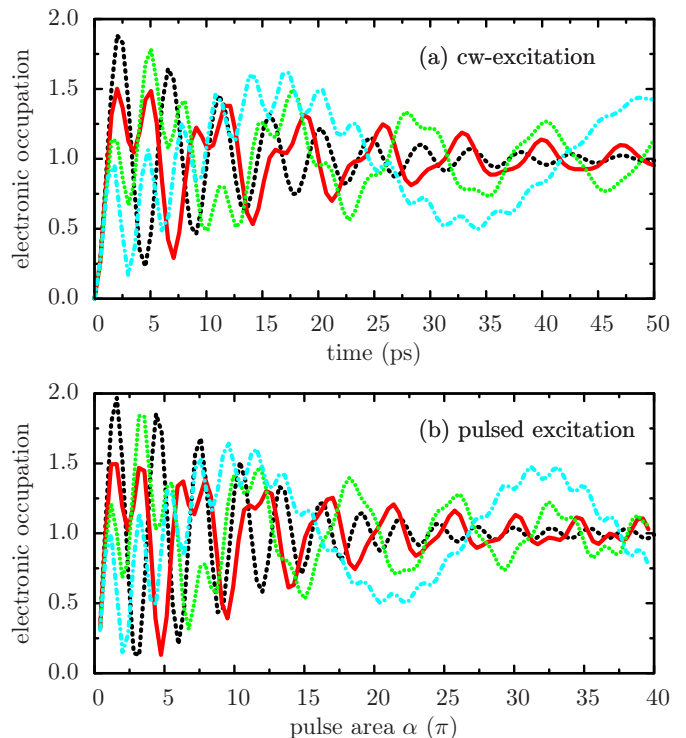


FIG. 3: (Color online) Totally created charge $C = C_E + 2C_B$ for different polarization parameters γ (see text): $\gamma = 1.0$ (black dashed line), 0.5 (red solid line), 0.3 (green dotted line), and 0.1 (blue dashed-dotted line) at $T = 10 \text{ K}$ and for $V_{\text{ex}} = \Delta = 0$. (a) shows the dynamics under cw-excitation for a total field strength of $f = 2.0 \text{ ps}^{-1}$ as a function of time, (b) displays the final QD occupation after a Gaussian shaped pulse with a FWHM of 30 ps as a function of the applied pulse area.

a very surprising finding. In light of a spin-independent exciton-phonon interaction one could rather expect that the damping is fully determined by the laser intensity and should thus depend only on f or other quantities related to the total intensity like $f_{\sigma_+} + f_{\sigma_-}$. However, our results clearly demonstrate that this is not the case and reveal a strong polarization dependence of the phonon-induced damping.

For the discussion of this remarkable finding, cw-excitations are most advantageous, as for this choice the field strengths $f_{\sigma_{\pm}}$ are time-independent and an analysis based on field-strength dependent damping rates as given below is particularly simple. However, in experiments it is a challenge to obtain time-resolved traces of the electronic occupation as presented in Fig. 3(a) and in most experimental studies pulsed excitations are used, where the final occupation is recorded as a function of the applied pulse area. We would like to stress, that the polarization dependence of the phonon-induced damping is also clearly seen for the latter scenario. This is exemplarily shown in Fig. 3(b), where the final occupation is plotted as a function of the pulse area for a Gaussian shaped pulse with a pulse duration of 30 ps (FWHM):

the reduction of the Rabi rotation amplitude with rising pulse area is the less the closer the polarization is to the circular limit, reflecting a decreased damping in the time domain.

The most convenient way to think of phonon-mediated relaxation is that the laser couples the excitonic states to form optically dressed states, that represent stable quasiparticles³³. As discussed in Sec. II C, the damping of Rabi oscillations is determined by the phonon spectral density evaluated at the transition frequencies between the dressed states, which for $\Delta = V_{\text{ex}} = 0$ are given by f_{σ_+} , f_{σ_-} , $f_{\sigma_+} - f_{\sigma_-}$ and $f_{\sigma_+} + f_{\sigma_-}$, but it turns out that terms involving $f_{\sigma_+} + f_{\sigma_-}$ or $f_{\sigma_+} - f_{\sigma_-}$ drop out. This result explains the strong dependence of the damping on the polarization seen in Fig. 3 as follows (for simplicity, we assume again cw-excitation): while for linear polarization both circularly polarized components are given by $f/\sqrt{2}$, for elliptical polarizations f_{σ_+} is larger and f_{σ_-} smaller than this value (without loss of generality we can assume f_{σ_+} to exceed f_{σ_-} , corresponding to $\gamma < 1$). Depending on the total laser intensity, we can then encounter two situations: either $J(f_{\sigma_-}) < J(f_{\sigma_+})$ and the σ_- driven subsystem experiences a weaker damping than in the case of an equally strong linear driving [which is fulfilled for the driving strength of $f = 2.0 \text{ ps}^{-1}$ in Fig. 3(a)], or $J(f_{\sigma_+}) < J(f_{\sigma_-})$ and the damping of the σ_+ driven subsystem is less strong. In any case, one subsystem experiences a weaker damping than in the linear case, which results in a weaker damping of the total electronic occupation, to which both subsystems contribute. From this reasoning it follows straightforwardly that for elliptically polarized excitations the difference of the damping compared to the linear case should monotonically increase with rising ellipticity, which is indeed confirmed by the results shown in Fig. 3.

For elliptical polarizations close to the circular limit, the carrier dynamics in one subsystem experiences eventually hardly any damping and C oscillates with large amplitudes over a long time-interval. In Fig. 3(a) this is nicely illustrated for $\gamma = 0.1$ (blue dashed-dotted line). First, the signal rapidly oscillates. However, after roughly 20 ps these fast oscillations have decayed. Subsequently, the dynamics changes qualitatively and is dominated by oscillations with a much longer period that are only weakly damped. While the fast oscillations reflect the dynamics in the σ_+ driven subsystem, the much less damped oscillations with a longer period stem from the σ_- driven subsystem. As for the chosen polarization f_{σ_-} is roughly ten times smaller than f_{σ_+} , the oscillations in the σ_- driven subsystem reveal a roughly ten times longer period and experience a considerably less damping, because here $J(f_{\sigma_-}) \ll J(f_{\sigma_+})$. This characteristic change in the dynamics is also expressed in corresponding results for pulsed excitations, cf. Fig. 3(b).

The limit of a strictly circular polarization with $\gamma = 0$ is special: for this excitation condition, one subsystem is driven with the total intensity, while the other subsystem is not driven at all. In consequence, while for

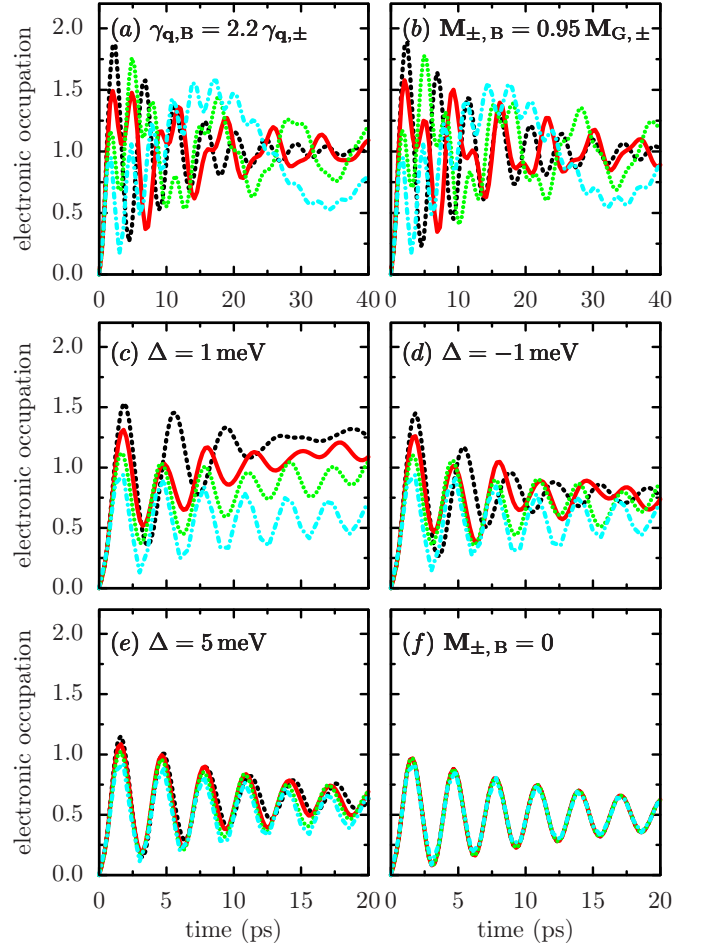


FIG. 4: (Color online) Totally created charge $C = C_E + 2C_B$ under cw-excitation as a function of time at $T = 10 \text{ K}$, $f = 2.0 \text{ ps}^{-1}$ and $V_{\text{ex}} = 0$ for different polarizations with $\gamma = 1.0$ (black dashed line), 0.5 (red solid line), 0.3 (green dotted line), and 0.1 (blue dashed-dotted line) for situations, in which the relevant damping rates do not separately depend on f_{σ_+} or f_{σ_-} (see text).

almost circularly polarized light the damping seen in the oscillations of the total occupation decreases with rising ellipticity and the time to become stationary rises without any limit for $\gamma \rightarrow 0$, this time is finite for circularly polarized light as discussed in more detail in Figs. 2(b) and (c) of Ref. 34.

It should be noted, that the finding that the damping rate depends separately on f_{σ_+} and f_{σ_-} strictly holds only in the strong confinement limit as defined by Eqs. (1)-(6) and in the limiting case $\Delta = V_{\text{ex}} = 0$ discussed so far. In the phonon-free case, it is easily seen that for $\Delta = V_{\text{ex}} = 0$ the model defined by Eqs. (1)-(6) can be decomposed into a product of two two-level systems, each evolving on its Bloch sphere with a Rabi frequency given by f_{σ_+} or f_{σ_-} , respectively. Thus, in this case we have two subsystems that evolve independently and react separately either on the values of f_{σ_+} or f_{σ_-} . In a four-level system composed of two independent two-level

systems each coupled to phonons, the phonon coupling of the two-exciton state must necessarily be twice the exciton-phonon coupling. Although this necessary condition is fulfilled in the exciton-biexciton system studied so far, we are actually not dealing with strictly independent dynamics on two Bloch-spheres as the two spheres are coupled to the same phonon modes. The resulting interdependence of the dynamics on the two Bloch spheres can be seen, e.g., from the fact that for linearly polarized driving the stationary biexciton occupation reached at long times is not given by $1/4$ (which would be the product of the stationary values of $1/2$ reached in any of the σ_{\pm} coupled two-level systems) but $1/3$.³⁴ Nevertheless, even though a strict factorization into two independently evolving subsystems does not hold, a phonon-coupling of the biexciton state $\gamma_{\mathbf{q},\text{B}}$ of exactly twice the exciton phonon-coupling $\gamma_{\mathbf{q},\pm}$ realizes a distinguished situation as in this case the phonon induced damping rates depend on f_{σ_+} and f_{σ_-} separately. However, this property is lost, when either $\gamma_{\mathbf{q},\text{B}} \neq 2\gamma_{\mathbf{q},\pm}$ or when the biexciton binding energy or the exchange interaction take finite values, or when the dipole moments associated with the ground state exciton transition $\mathbf{M}_{\text{G},\pm}$ and the exciton biexciton transition $\mathbf{M}_{\pm,\text{B}}$ are different. In each of these cases terms involving $f_{\sigma_+} + f_{\sigma_-}$ or $f_{\sigma_+} - f_{\sigma_-}$ enter the equations derived within the weak coupling theory. It turns out, however, that for many typical situations with deviations from the limiting case discussed so far, the amplitudes of the additional terms are small and the polarization dependence is still close to the results shown in Fig. 3. This is illustrated in Fig. 4 and shall be discussed in the remainder of the paper.

In real systems, $\mathbf{M}_{\pm,\text{B}}$ differs from $\mathbf{M}_{\text{G},\pm}$ due to deviations from the strict strong confinement limit, where the multi-pair wave functions factorize in single particle wave functions for electrons and holes. Typical values observed in experiments indicate, that $\mathbf{M}_{\pm,\text{B}}$ is roughly 5% smaller than $\mathbf{M}_{\text{G},\pm}$.^{31,51} For the same reason, $\gamma_{\mathbf{q},\text{B}} \neq 2\gamma_{\mathbf{q},\pm}$ is possible. Figs. 4(a) and 4(b) show results for calculations assuming $\mathbf{M}_{\pm,\text{B}} = 0.95\mathbf{M}_{\text{G},\pm}$ and $\gamma_{\mathbf{q},\text{B}} = 2.2\gamma_{\mathbf{q},\pm}$, respectively, for the same polarizations as in Fig. 3. It is clearly seen that the polarization dependence is only weakly influenced by these deviations from the strong confinement limit.

We have also performed calculations (not shown) accounting for a finite exchange interaction of $V_{\text{ex}} = 30\mu\text{eV}$, which represents a typical value. Although V_{ex} yields a direct coupling of the two subspaces driven by σ_{\pm} polarized light, we found only very small changes compared to $V_{\text{ex}} = 0$, except for strict circular polarization³⁴ or in the regime of nearly circularly polarized excitations, when the time-scale on which the total system is driven to a stationary state increases drastically and exceeds h/V_{ex} .

Finally, let us turn to the influence of finite values of the biexciton binding energy, as illustrated in Figs. 4(c) and 4(d) for $\Delta = 1.0$ and -1.0 meV, respectively. At first one may notice that the mean value of the oscilla-

tions decreases with rising ellipticity of the polarization. This lowering of the total signal is due to the fact, that the biexciton generation becomes more unlikely, when f_{σ_-} decreases, as in this case the exciton biexciton transition given an exciton generated by σ_+ polarized light becomes less probable. In addition, there is no longer a cross-over between fast and slow oscillations for almost circularly polarized excitations. However, despite these differences compared to the case of a vanishing biexciton binding energy, we find a very similar behavior as discussed so far: the decay of the oscillation amplitude is the less pronounced the more far the excitation is from the linear case, clearly illustrating a strong dependence of the phonon-induced damping on the polarization of the driving laser light. This picture changes, however, for larger Δ , which are still feasible, as shown in Fig. 4(e) for $\Delta = 5$ meV. Here, the polarization dependence is drastically suppressed. As the coupling to the biexciton decreases with rising Δ , this indicates, that an efficient coupling to the biexciton is of fundamental importance for the polarization dependence of the damping. Indeed, when we completely decouple the biexciton from the dynamics by setting by hand $\mathbf{M}_{\pm,\text{B}} = 0$, then the polarization dependence vanishes altogether and the phonon-induced damping is fully determined by the pulse intensity [cf. Fig. 4(f), where all four lines coincide]. Only when the biexciton is coupled, there is the possibility to essentially drive two different Bloch spheres with individual Rabi frequencies within the four-level system considered here, giving rise to the polarization dependence of the phonon-induced damping as explained above.

IV. CONCLUSIONS

In summary, we have presented a numerically complete analysis of the phonon impact on optically driven exciton-biexciton QD systems. Rabi rotation scenarios for finite biexciton binding energies were shown to differ significantly from the two-level case and offer manifold insights in the dynamics of an exciton-biexciton system, including the interplay between off-resonant driving and quantum dissipative relaxation. In addition, we have demonstrated that although the carrier-phonon interaction is independent of the spin, the phonon-induced damping does not only depend on the pulse intensity but is for typical parameters also strongly affected by the polarization of the driving laser pulse. While the damping is strongest for linearly polarized excitations, it is the more reduced the closer the polarization is to the circular limit. For almost circularly polarized excitations and small biexciton binding energies, the Rabi scenario changes strongly in the course of time reflecting different dynamics in the σ_{\pm} driven subsystems. The origin of the polarization dependent phonon-induced damping is the possibility to drive two Bloch spheres essentially each with its own Rabi-frequency $f_{\sigma_{\pm}}$ that are determined by the polarization, together with the fact that

it is the Rabi frequency that determines the damping in a two-level system. This possibility is intimately related to an efficient coupling to the biexciton state, which highlights the pivotal role of this two-pair state for the discussed dynamics.

V. ACKNOWLEDGMENTS

M. G. gratefully acknowledges financial support by the Studienstiftung des Deutschen Volkes. We also highly appreciate many fruitful discussions with T. Kuhn.

VI. APPENDIX

In this appendix, we give a short description of the weak coupling theory presented in Sec. II C concentrating on the limit of strong electronic confinement as defined by Eqs. (1)-(6) and the special case $\Delta = V_{\text{ex}} = 0$. The Heisenberg equations of motion for the electronic operators $\hat{\rho}_{ij} = |d_i\rangle\langle d_j|$ read

$$\partial_t \hat{\rho}_{ij} = \frac{i}{\hbar} [H, \hat{\rho}_{ij}], \quad (10)$$

where the overbar indicates, that we are working in the dressed state basis. By taking expectation values we obtain equations of motion for the elements of the reduced density matrix $\bar{\rho}_{ij} = \langle \hat{\rho}_{ij} \rangle$, where single phonon assisted density matrix elements of the form $\langle \hat{\rho}_{i,j} b_{\mathbf{q}}^\dagger \rangle$ or $\langle \hat{\rho}_{i,j} b_{\mathbf{q}} \rangle$ enter. Setting up equations of motion for these single phonon assisted quantities, in turn, introduces double phonon assistances. In order to truncate the resulting hierarchy of higher order phonon assisted quantities, we set

$$\langle \hat{\rho}_{ij} b_{\mathbf{q}}^\dagger b_{\mathbf{q}'} \rangle = \bar{\rho}_{ij} \langle b_{\mathbf{q}}^\dagger b_{\mathbf{q}'} \rangle = \bar{\rho}_{ij} n_{\mathbf{q}} \delta_{\mathbf{q},\mathbf{q}'} \quad (11a)$$

$$\langle \hat{\rho}_{ij} b_{\mathbf{q}} b_{\mathbf{q}'}^\dagger \rangle = \bar{\rho}_{ij} \langle b_{\mathbf{q}} b_{\mathbf{q}'}^\dagger \rangle = \bar{\rho}_{ij} (n_{\mathbf{q}} + 1) \delta_{\mathbf{q},\mathbf{q}'} \quad (11b)$$

$$\langle \hat{\rho}_{ij} b_{\mathbf{q}} b_{\mathbf{q}'} \rangle = \langle \hat{\rho}_{ij} b_{\mathbf{q}}^\dagger b_{\mathbf{q}'}^\dagger \rangle = 0, \quad (11c)$$

where $n_{\mathbf{q}} = 1/(\exp(\hbar\omega_{\mathbf{q}}/k_B T) - 1)$ denotes the Bose-Einstein occupancy at temperature T . By doing so, one obtains for the single phonon assisted elements a set of closed equations. Exemplarily, we have

$$\begin{aligned} \partial_t \langle \hat{\rho}_{12} b_{\mathbf{q}} \rangle &= i(-\omega_{\mathbf{q}} + \lambda_{21}) \langle \hat{\rho}_{12} b_{\mathbf{q}} \rangle \\ &+ \frac{i\gamma_{\mathbf{q}}}{2} [-2\bar{\rho}_{12} - n_{\mathbf{q}}(\bar{\rho}_{22} + \bar{\rho}_{42}) \\ &+ (n_{\mathbf{q}} + 1)(\bar{\rho}_{11} + \bar{\rho}_{13})]. \end{aligned} \quad (12)$$

Integrating these equations yields integrals of the form

$$\int_0^\infty \exp(i\omega\tau) \bar{\rho}_{ij}(t - \tau) d\tau. \quad (13)$$

Next, we perform a Markov approximation by identifying slowly varying variables and taking them out of these

memory integrals. While occupations can be regarded as slowly varying, this is usually not the case for coherences, that are generally rapidly changing quantities. However, as their free oscillation frequency is given by $\lambda_{ji} := \lambda_j - \lambda_i$, we can set $\bar{\rho}_{ij}(t) = \exp(i\lambda_{ji}t) \tilde{\bar{\rho}}_{ij}(t)$, where $\tilde{\bar{\rho}}_{ij}(t)$ can be expected to vary slowly. Taking these variables out of the integral yields

$$\int_0^\infty \exp(i\omega\tau) \bar{\rho}_{ij}(t - \tau) d\tau = \bar{\rho}_{ij}(t) \int_0^\infty \exp[i(\omega - \lambda_{ji})\tau] d\tau \quad (14)$$

and the remaining integrals can be easily evaluated using

$$\int_0^\infty \exp(i\omega\tau) d\tau = \pi\delta(\omega) + i\frac{P}{\omega}, \quad (15)$$

where P denotes Cauchy's principal value. It is well known that the principal value terms only lead to a small renormalization of the system Hamiltonian but do not directly contribute to dephasing.⁴⁵ Therefore, we neglect these terms and obtain:

$$\begin{aligned} \langle \hat{\rho}_{12} b_{\mathbf{q}} \rangle &= \frac{i\pi\gamma_{\mathbf{q}}}{2} [-2\bar{\rho}_{12}\delta(\omega_{\mathbf{q}}) - n_{\mathbf{q}}\bar{\rho}_{22}\delta(\omega_{\mathbf{q}} + \lambda_{12}) \\ &- n_{\mathbf{q}}\bar{\rho}_{42}\delta(\omega_{\mathbf{q}} + \lambda_{14}) \\ &+ (n_{\mathbf{q}} + 1)\bar{\rho}_{11}\delta(\omega_{\mathbf{q}} + \lambda_{12}) \\ &+ (n_{\mathbf{q}} + 1)\bar{\rho}_{13}\delta(\omega_{\mathbf{q}} - \lambda_{23})]. \end{aligned} \quad (16)$$

Here, only $\lambda_{14} = \lambda_{23} = f_{\sigma_+}$ and $\lambda_{12} = \lambda_{43} = f_{\sigma_-}$ appear, although in Eq. (12) also combinations like $\lambda_{24} = f_{\sigma_+} - f_{\sigma_-}$ (via the free oscillation of $\langle \bar{\rho}_{42} \rangle$) entered, because the corresponding contributions cancel out. It is an important point to note, that this holds for all other phonon-assisted density matrix elements as well: from here on only $\delta(\omega - f_{\sigma_+})$ and $\delta(\omega - f_{\sigma_-})$ enter the resulting equations. Terms involving $\delta[\omega - (f_{\sigma_+} + f_{\sigma_-})]$ or $\delta[\omega - (f_{\sigma_+} - f_{\sigma_-})]$ are absent due to the structure of $H_{\text{dot-light}}$ and $H_{\text{dot-phonon}}$ in the special case considered here. Introducing the phonon spectral density

$$J(\omega) = \sum_{\mathbf{q}} \gamma_{\mathbf{q}}^2 \delta(\omega - \omega_{\mathbf{q}}) \quad (17)$$

and substituting the expressions for the single phonon assisted density matrix elements into Eq. (10) eventually leads to a closed set of equations of motion for the elements of the reduced electronic density matrix.

We mention, that the weak coupling theory derived here yields the same result as a four-level extension of the master-equation approach that has been presented in Ref. 4 for the case of an electronic two-level system. For two-level systems the latter approach has been compared to a much more advanced variational master-equation approach in Ref. 6, which in turn has been shown to agree well with numerically exact path integral calculations for not too high temperatures and standard GaAs parameters, that represent a weak carrier-phonon coupling regime. We checked that in the four-level case, the

deviations of the weak coupling theory to numerically exact calculations are qualitatively similar as in the two-level case and refer to Ref. 6 for a comparison. Readers interested in the validity ranges of approximate methods in the regimes of strong carrier-phonon couplings or high temperatures are referred to Refs. 33 and 52,

where path integral calculations have been compared to a second-order and fourth-order correlation expansion, clearly demonstrating the superiority of a numerically exact approach, accounting fully for all non-Markovian effects and arbitrary multiphonon processes.

-
- * martin.glaessl@uni-bayreuth.de
- ¹ S. M. Ulrich, S. Ates, S. Reitzenstein, A. Löffler, A. Forchel, and P. Michler, *Phys. Rev. Lett.* **106**, 247402 (2011).
 - ² C. Roy and S. Hughes, *Phys. Rev. Lett.* **106**, 247403 (2011).
 - ³ A. Vagov, M. D. Croitoru, V. M. Axt, T. Kuhn, and F. M. Peeters, *Phys. Rev. Lett.* **98**, 227403 (2007).
 - ⁴ A. J. Ramsay, A. V. Gopal, E. M. Gauger, A. Nazir, B. W. Lovett, A. M. Fox, and M. S. Skolnick, *Phys. Rev. Lett.* **104**, 017402 (2010).
 - ⁵ A. J. Ramsay, T. M. Godden, S. J. Boyle, E. M. Gauger, A. Nazir, B. W. Lovett, A. M. Fox, and M. S. Skolnick, *Phys. Rev. Lett.* **105**, 177402 (2010).
 - ⁶ D. P. S. McCutcheon, N. S. Dattani, E. M. Gauger, B. W. Lovett, and A. Nazir, *Phys. Rev. B* **84**, 081305 (2011).
 - ⁷ A. Ulhaq, S. Weiler, S. M. Ulrich, R. Roßbach, M. Jetter, and P. Michler, *Nature Photonics* **6**, 238 (2012).
 - ⁸ P. Kaer, T. R. Nielsen, P. Lodahl, A. P. Jauho, and J. Mørk, *Phys. Rev. Lett.* **104**, 157401 (2010).
 - ⁹ Y. Wu, I. M. Piper, M. Ediger, P. Brereton, E. R. Schmidgall, P. R. Eastham, M. Hugues, M. Hopkinson, and R. T. Phillips, *Phys. Rev. Lett.* **106**, 067401 (2011).
 - ¹⁰ C. M. Simon, T. Belhadj, B. Chatel, T. Amand, P. Renucci, A. Lemaitre, O. Krebs, P. A. Dalgarno, R. J. Warburton, X. Marie, et al., *Phys. Rev. Lett.* **106**, 166801 (2011).
 - ¹¹ M. Glässl, L. Sörgel, A. Vagov, M. D. Croitoru, T. Kuhn, and V. M. Axt, *Phys. Rev. B* **86**, 035319 (2012).
 - ¹² O. Benson, C. Santori, M. Pelton, and Y. Yamamoto, *Phys. Rev. Lett.* **84**, 2513 (2000).
 - ¹³ O. Gywat, G. Burkard, and D. Loss, *Phys. Rev. B* **65**, 205329 (2002).
 - ¹⁴ U. Hohenester, *Phys. Rev. B* **66**, 245323 (2002).
 - ¹⁵ A. Dousse, J. Suffczynski, A. Beveratos, O. Krebs, A. Lemaitre, I. Sagnes, J. Bloch, P. Voisin, and P. Senellart, *Nature* **466**, 217 (2010).
 - ¹⁶ F. Troiani, U. Hohenester, and E. Molinari, *Phys. Rev. B* **62**, R2263 (2000).
 - ¹⁷ E. Biolatti, R. C. Iotti, P. Zanardi, and F. Rossi, *Phys. Rev. Lett.* **85**, 5647 (2000).
 - ¹⁸ P. Chen, C. Piermarocchi, and L. J. Sham, *Phys. Rev. Lett.* **87**, 067401 (2001).
 - ¹⁹ B. Krummheuer, V. M. Axt, and T. Kuhn, *Phys. Rev. B* **65**, 195313 (2002).
 - ²⁰ P. Borri, W. Langbein, S. Schneider, U. Woggon, R. L. Sellin, D. Ouyang, and D. Bimberg, *Phys. Rev. B* **66**, 081306(R) (2002).
 - ²¹ A. Vagov, V. M. Axt, T. Kuhn, W. Langbein, P. Borri, and U. Woggon, *Phys. Rev. B* **70**, 201305(R) (2004).
 - ²² J. Förstner, C. Weber, J. Danckwerts, and A. Knorr, *Phys. Rev. Lett.* **91**, 127401 (2003).
 - ²³ P. Machnikowski and L. Jacak, *Phys. Rev. B* **69**, 193302 (2004).
 - ²⁴ A. Krügel, V. M. Axt, T. Kuhn, P. Machnikowski, and A. Vagov, *Appl. Phys. B* **81**, 897 (2005).
 - ²⁵ V. M. Axt, P. Machnikowski, and T. Kuhn, *Phys. Rev. B* **71**, 155305 (2005).
 - ²⁶ T. E. Hodgson, L. Viola, and I. D'Amico, *Phys. Rev. B* **78**, 165311 (2008).
 - ²⁷ S. Lüker, K. Gawarecki, D. E. Reiter, A. Grodecka-Grad, V. M. Axt, P. Machnikowski, and T. Kuhn, *Phys. Rev. B* **85**, 121302 (2012).
 - ²⁸ M. Glässl, M. D. Croitoru, A. Vagov, V. M. Axt, and T. Kuhn, *Phys. Rev. B* **84**, 125304 (2011).
 - ²⁹ V. M. Axt, T. Kuhn, A. Vagov, and F. M. Peeters, *Phys. Rev. B* **72**, 125309 (2005).
 - ³⁰ A. Krügel, A. Vagov, V. M. Axt, and T. Kuhn, *Phys. Rev. B* **76**, 195302 (2007).
 - ³¹ S. Stuffer, P. Machnikowski, P. Ester, M. Bichler, V. M. Axt, T. Kuhn, and A. Zrenner, *Phys. Rev. B* **73**, 125304 (2006).
 - ³² P. Machnikowski, *Phys. Rev. B* **78**, 195320 (2008).
 - ³³ M. Glässl, A. Vagov, S. Lüker, D. E. Reiter, M. D. Croitoru, P. Machnikowski, V. M. Axt, and T. Kuhn, *Phys. Rev. B* **84**, 195311 (2011).
 - ³⁴ M. Glässl, M. D. Croitoru, A. Vagov, V. M. Axt, and T. Kuhn, *Phys. Rev. B* **85**, 195306 (2012).
 - ³⁵ G. D. Mahan, *Many-Particle Physics* (Plenum Press, New York, 1990), 2nd ed.
 - ³⁶ E. Peter, J. Hours, P. Senellart, A. Vasanelli, A. Cavanna, J. Bloch, and J. M. Gérard, *Phys. Rev. B* **69**, 041307(R) (2004).
 - ³⁷ L. Allen and J. H. Eberly, *Optical Resonance and Two-Level Atoms* (John Wiley and Sons, New York, 1975).
 - ³⁸ A. Vagov, M. D. Croitoru, M. Glässl, V. M. Axt, and T. Kuhn, *Phys. Rev. B* **83**, 094303 (2011).
 - ³⁹ N. Makri and D. Makarov, *J. Chem. Phys.* **102**, 4600 (1995).
 - ⁴⁰ N. Makri and D. Makarov, *J. Chem. Phys.* **102**, 4611 (1995).
 - ⁴¹ M. Thorwart, P. Reimann, and P. Hänggi, *Phys. Rev. E* **62**, 5808 (2000).
 - ⁴² P. Nalbach and M. Thorwart, *Phys. Rev. B* **81**, 054308 (2010).
 - ⁴³ E. Sim, *J. Chem. Phys.* **115**, 4450 (2001).
 - ⁴⁴ F. Rossi and T. Kuhn, *Rev. Mod. Phys.* **74**, 895 (2002).
 - ⁴⁵ H. P. Breuer and F. Petruccione, *The Theory of Open Quantum Systems* (Oxford University Press, Oxford, 2002), 1st ed.
 - ⁴⁶ A. Vagov, M. D. Croitoru, V. M. Axt, T. Kuhn, and F. M. Peeters, *Phys. Status Solidi B* **243**, 2233 (2006).
 - ⁴⁷ A. M. Weiner, *Progr. Quantum Electron.* **19**, 161 (1995).
 - ⁴⁸ E. T. Jaynes and F. W. Cummings, *Proc. IEEE* **51**, 89 (1963).
 - ⁴⁹ A. Zrenner, E. Beham, S. Stuffer, F. Findeis, M. Bichler,

- and G. Abstreiter, *Nature* **418**, 612 (2002).
- ⁵⁰ M. Zecherle, C. Ruppert, E. C. Clark, G. Abstreiter, J. J. Finley, and M. Betz, *Phys. Rev. B* **82**, 125314 (2010).
- ⁵¹ S. J. Boyle, A. J. Ramsay, F. Bello, H. Y. Liu, M. Hopkinson, A. M. Fox, and M. S. Skolnick, *Phys. Rev. B* **78**, 075301 (2008).
- ⁵² A. Vagov, M. D. Croitoru, V. M. Axt, P. Machnikowski, and T. Kuhn, *Phys. Status Solidi B* **248**, 839 (2011).